# Chapter 5

# Experimental Results

## 5.1 Introduction

Acoustic and other characteristics of the developed materials will be presented in this chapter. Particular attention will be paid to the relations between the non-acoustic and acoustic characteristics of the extruded materials in an attempt to characterise fully the acoustical performance of these materials. All products were tested at 30mm thickness and material properties of six specimens for each of the manufactured materials were analysed to check for homogeneity, these absorption coefficient results are presented in section 5.7 with the standard deviations.

## 5.2 Waste used in the experimental trials

The following type of waste was used in this work:

i. Tyre shred residue
ii. Car dashboard crumb
iii. PVC backed carpet waste

Used tyres constitute a great proportion of total automotive waste. Tyres are granulated and separated into various grain sizes. Although the resultant rubber granular mix can be recycled, there is a considerable amount of waste left over during the granulation process. This waste is called tyre shred residue (rayon), approximately 100 tonnes of

rayon is produced per week by a single tyre granulating company based in Yorkshire. The company has no use for this waste and is sent to the landfill. Manufacturing companies are looking at technologies to recycle their own manufacturing waste like tyre shred residue.

Tyre shred residue Car dashboard crumb

**Figure 5.1**: Tyre shred residue and car dashboard crumb used in the experiments

Rayon consists of rubber grains mixed with fibres (Figure 5.1) and the size of the grains in this mix is below 5mm. The shape of the grains is irregular, which results in the relatively high open porosity and, therefore, high values of acoustic absorption. The fibre length ranges from 1mm to 20mm, after separation of rayon using the cyclone, the proportion of fibres to grain by weight was 20%: 80% respectively. After the separation some rubber grains had a small amount of fibres attached to the grains so that it was not possible to completely separate the fibrous and granular components. Other wastes used in the experiments were PVC backed carpet tiles (Figure 5.2), which was granulated and separated into fibres and grains using the same cyclone separation technology. In addition, the car dashboard crumb was used. It came already granulated and required no further processing.

**Figure 5.2**: Defected PVC backed carpet tile (left) and trimming (right)

## 5.3 Calibration of the extruder

The binder setting for the extrusion process was calculated from the calibration graph using the following procedure. To obtain the binder vessel pressure setting for $V_B$ amount of binder, we use the line equation from the calibration graph (Figure 5.3):

$$Q_m = 0.98V_B - 3 \tag{5.1}$$

then the binder setting was $V_B = (Q_m + 3)/0.98$, where $Q_m$ is the flow rate of the binder. Figure 5.3 shows the linear behaviour of the MDI binder calibration graph; Table 5.1 shows the calibration data.

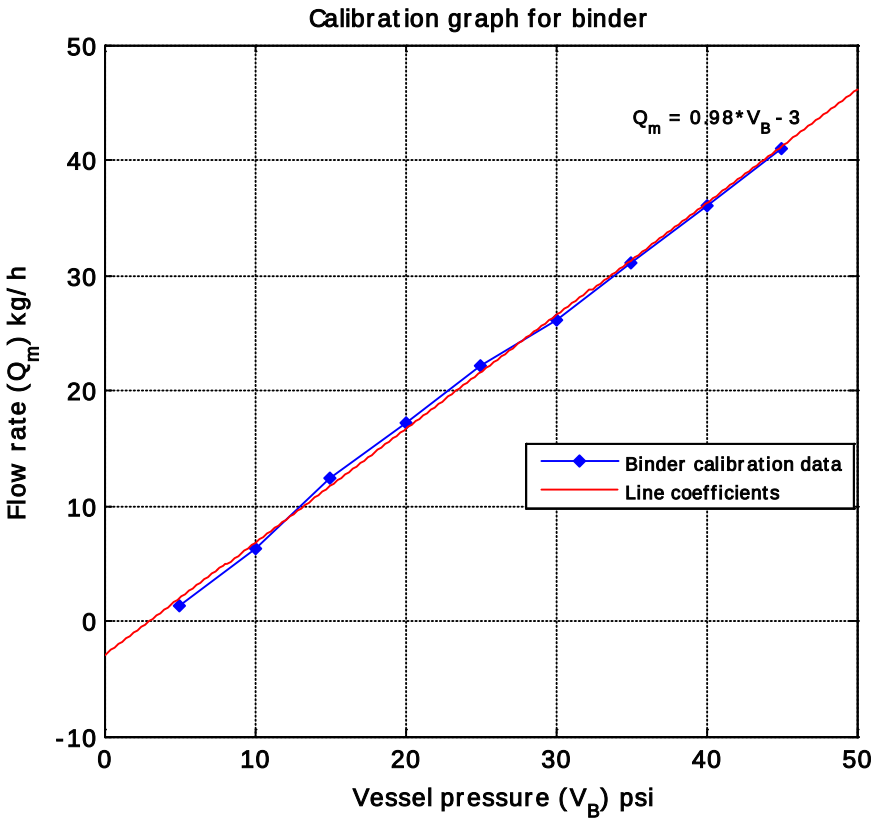


**Figure 5.3**: Calibration graph of MDI binder

**Table 5.1**: Calibration data for the binder

| Vessel pressure (psi) | Weight of binder (g) | Time (sec.) | Flow rate (kg/hr) |
|---|---|---|---|
| 5 | 22.2 | 60 | 1.33 |
| 10 | 105.7 | 60 | 6.34 |
| 15 | 206.3 | 60 | 12.38 |
| 20 | 287 | 60 | 17.22 |
| 25 | 370 | 60 | 22.18 |
| 30 | 436 | 60 | 26.15 |
| 35 | 518.5 | 60 | 31.11 |
| 40 | 601.3 | 60 | 36.08 |
| 45 | 684.2 | 60 | 41.05 |

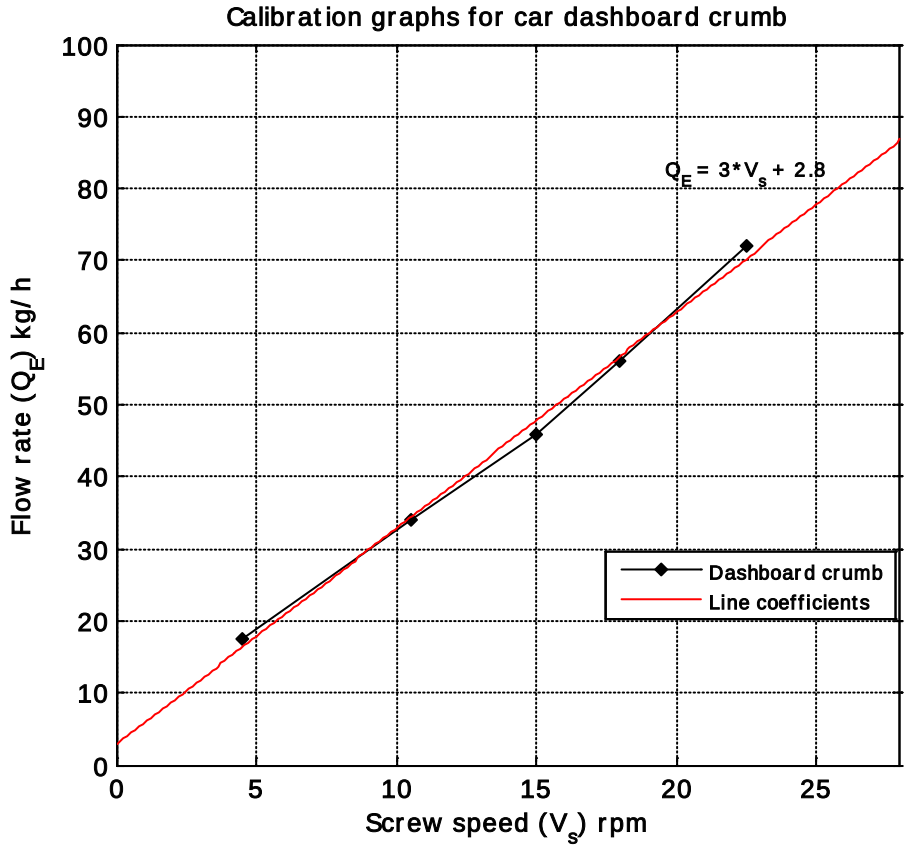


**Figure 5.4**: Calibration graph for car dashboard

Figure 5.4 shows the linear behaviour of the mass calibration of car dashboard crumb; Table 5.2 shows the calibration data.

**Table 5.2**: Calibration data for the car dashboard crumb

| Screw speed (Hz) | Revolutions per minute (rpm) | Weight of crumb (g) | Time (sec.) | Flow rate (kg/hr) |
|---|---|---|---|---|
| 3 | 4.5 | 920.1 | 180 | 18.4 |
| 7 | 10.5 | 1675.9 | 180 | 33.5 |
| 10 | 15 | 2315.4 | 180 | 46.3 |
| 12 | 18 | 2810.3 | 180 | 56.2 |
| 15 | 22.5 | 3550.6 | 180 | 71 |

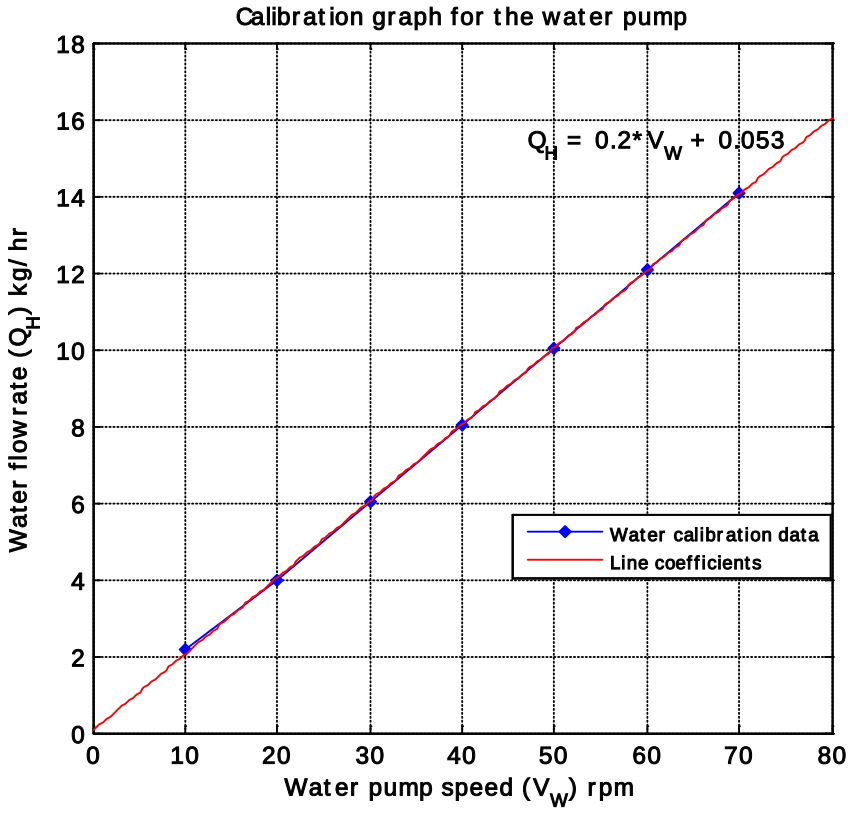


**Figure 5.5**: Calibration graph for water pump

Figure 5.5 shows the linear behaviour for the water pump, and Table 5.3 shows the calibration data.

**Table 5.3**: Calibration data for the water pump

| Pump speed (rpm) | Weight of water (g) | Time (sec.) | Flow rate (kg/hr) |
|---|---|---|---|
| 10 | 36.1 | 60 | 2.16 |
| 20 | 66.1 | 60 | 3.96 |
| 30 | 100.6 | 60 | 6.03 |
| 40 | 133.5 | 60 | 8.01 |
| 50 | 167.4 | 60 | 10.04 |
| 60 | 201.4 | 60 | 12.08 |
| 70 | 234.5 | 60 | 14.07 |

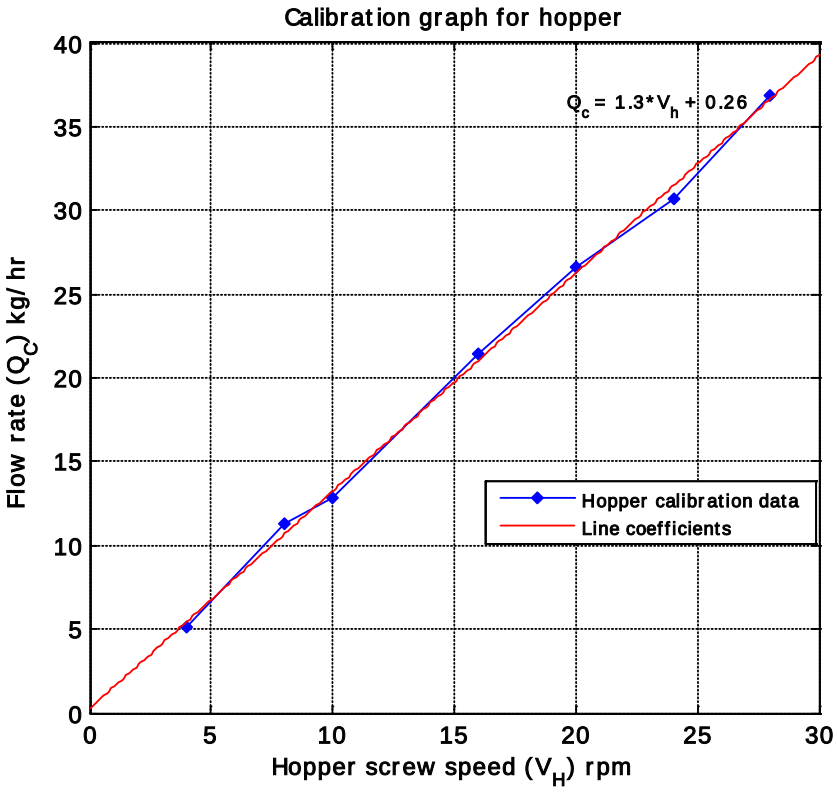


**Figure 5.6**: Calibration graph for hopper

Figure 5.6 shows the linear behaviour for the hopper calibration graph; Table 5.4 shows the calibration data.

**Table 5.4**: Calibration data for the hopper

| Hopper screw speed (rpm) | Weight of granules (g) | Time (sec.) | Flow rate (kg/hr) |
|---|---|---|---|
| 4 | 85.3 | 60 | 5.12 |
| 8 | 187.3 | 60 | 11.24 |
| 10 | 213.3 | 60 | 12.8 |
| 16 | 358 | 60 | 21.48 |
| 20 | 443 | 60 | 26.6 |
| 24 | 512 | 60 | 30.72 |
| 28 | 614 | 60 | 36.84 |

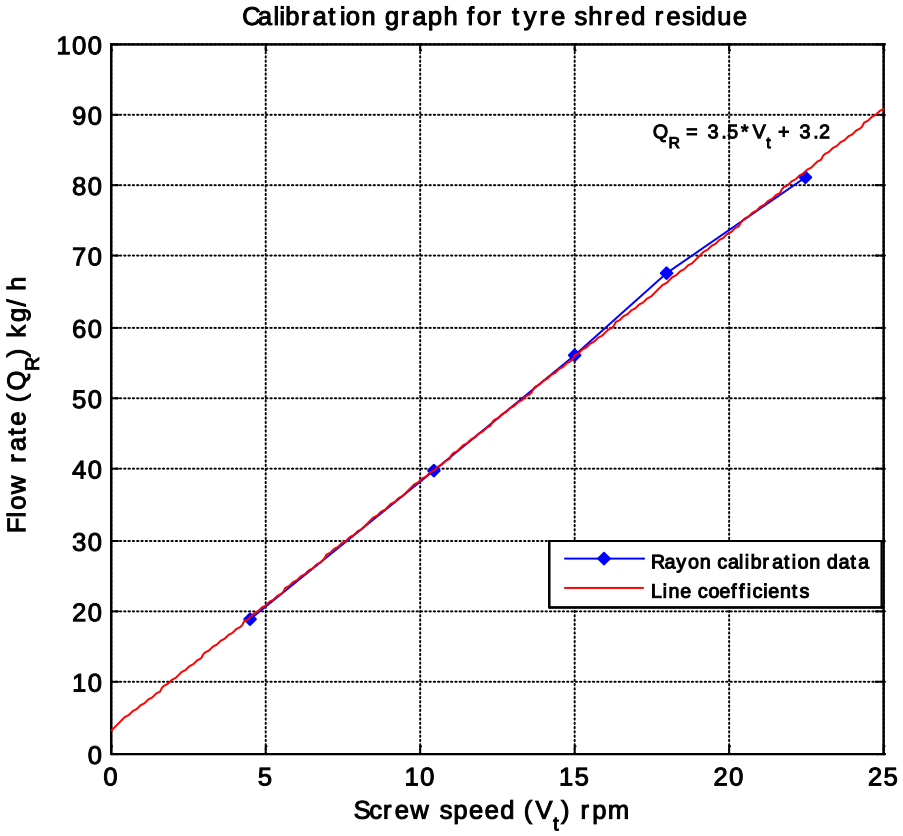


**Figure 5.7**: Calibration graph for tyre shred residue

**Table 5.5**: Calibration data for the tyre shred residue

| Screw speed (Hz) | Revolutions per minute (rpm) | Weight of rayon (g) | Time (sec.) | Flow rate (kg/hr) |
|---|---|---|---|---|
| 3 | 4.5 | 937.5 | 180 | 18.75 |
| 7 | 10.5 | 1987.5 | 180 | 39.75 |
| 10 | 15 | 2800 | 180 | 56 |
| 12 | 18 | 3377 | 180 | 67.54 |
| 15 | 22.5 | 4050 | 180 | 81 |

Figures 5.7 shows the linear behaviour of the calibration graph for tyre shred residue, and Table 5.5 provides the calibration data.

The flow rates quoted here were measured using weight not volume from the extruder calibration graphs as shown in equations 5.3 to 5.8. For this purpose three calibration graphs of the following variables were needed:

i. Waste material calibration graph
ii. Binder calibration graph
iii. Water calibration graph

Procedure for setting the extruder for an experiment:

For a total flow rate of $Q_r$, the main screw speed was selected from the calibration graph. Then percentage composition of the variables was selected based on a particular formulation, e.g. 50% rayon, 30% binder, and 20% water.

If percentage rayon in the formulation was 50%, and mass flow rate for rayon was $Q_R$, then,

$$\frac{Q_R}{Q_r} \times 100 = 50\% \tag{5.2}$$

$$Q_w = \frac{50}{100} \times Q_r = kg/h \tag{5.3}$$

Then from the calibration graph of rayon the speed for $Q_R$ kg/h flow rate can be set based on the total flow rate $Q_r$.

If percentage binder in the mix was 30%, and mass flow rate for binder was $Q_B$, then:

$$\frac{Q_B}{Q_r} \times 100 = 30\% \tag{5.4}$$

$$Q_B = \frac{30}{100} \times Q_r = kg/h \tag{5.5}$$

Then from the calibration graph of binder the speed setting for $Q_B$ kg/h flow rate can be set.

If percentage water in the mix was 20%, and mass flow rate in barrel of water was $Q_H$, then:

$$\frac{Q_H}{Q_r} \times 100 = 20\% \tag{5.6}$$

$$Q_H = \frac{20}{100} \times Q_r = kg/h \tag{5.7}$$

Then from the calibration graph of water the speed setting for $Q_H$ kg/h flow rate can be selected. The total mass flow rates of the rayon, binder and water should add up to $Q_r$ kg/h.

## 5.4 Influence of extruder variables on the acoustical performance of materials

From the preliminary experiments on the prototype extruder, it was decided to use the optimised parameters shown in Table 5.6. The screw speed was kept constant at 10 rpm to give the material the right residence time in the barrel, along with a corresponding reduction in the hopper feed rate to maintain an equivalent channel fill fraction. The target output was maintained at 8 kg/h. The percentage binder used in the experiments was 50% by weight and water was 10% by weight.

**Table 5.6**: Default values of controlled factors for the prototype extruder

| Variables | Value |
|---|---|
| Flow rate (kg/h) | 8 |
| Screw speed (rpm) | 10 |
| Percentage binder | 50 |
| Percentage water | 10 |
| Fibre length (mm) | 2.0-4.0 |
| Grain size (mm) | 1.0-2.0 |
| Percentage of grain | 24 |
| Percentage of fibre | 16 |

The impact of the above features on the performance of the extruded materials will be described in this section, by changing key variables whilst holding other variables constant on the prototype extruder materials having variable properties were produced, the variables that were changed are presented in Table 5.7.

**Table 5.7**: Prototype extruder variables that were changed (design of experiments) for PVC backed carpet waste stream

| | Variables | | | | | Protoype extruder variables | |
|---|---|---|---|---|---|---|---|
| Sample | Binder level (%) | Fibre to grain ratio | Grain size (mm) | Fibre length (mm) | Water : Binder | Screw speed(rpm) | Flow rate (kg/h) |
| LM10 | 10 | 40-60 | 2.0-4.0 | 2.0-4.0 | 1 to 5 | 10 | 8 |
| LM11 | 20 | 40-60 | 2.0-4.0 | 2.0-4.0 | 1 to 5 | 10 | 8 |
| LM12 | 30 | 40-60 | 2.0-4.0 | 2.0-4.0 | 1 to 5 | 10 | 8 |
| LM13 | 40 | 40-60 | 2.0-4.0 | 2.0-4.0 | 1 to 5 | 10 | 8 |
| LM14 | 50 | 40-60 | 2.0-4.0 | 2.0-4.0 | 1 to 5 | 10 | 8 |
| LM15 | 30 | 20-80 | 2.0-4.0 | 2.0-4.0 | 1 to 5 | 10 | 8 |
| LM16 | 30 | 40-60 | 2.0-4.0 | 2.0-4.0 | 1 to 5 | 10 | 8 |
| LM17 | 30 | 60-40 | 2.0-4.0 | 2.0-4.0 | 1 to 5 | 10 | 8 |
| LM18 | 30 | 80-20 | 2.0-4.0 | 2.0-4.0 | 1 to 5 | 10 | 8 |
| LM19 | 30 | 100-0 | 2.0-4.0 | 2.0-4.0 | 1 to 5 | 10 | 8 |
| LM20 | 30 | 40-60 | <0.5 | 2.0-4.0 | 1 to 5 | 10 | 8 |
| LM21 | 30 | 40-60 | 0.5-1.0 | 2.0-4.0 | 1 to 5 | 10 | 8 |
| LM22 | 30 | 40-60 | 1.0-2.0 | 2.0-4.0 | 1 to 5 | 10 | 8 |
| LM23 | 30 | 40-60 | 2.0-4.0 | 2.0-4.0 | 1 to 5 | 10 | 8 |
| LM24 | 30 | 40-60 | >5 | 2.0-4.0 | 1 to 5 | 10 | 8 |
| LM25 | 30 | 40-60 | 2.0-4.0 | <1 | 1 to 5 | 10 | 8 |
| LM26 | 30 | 40-60 | 2.0-4.0 | 2.0-4.0 | 1 to 5 | 10 | 8 |
| LM27 | 30 | 40-60 | 2.0-4.0 | 4.0-5.0 | 1 to 5 | 10 | 8 |
| LM28 | 30 | 40-60 | 2.0-4.0 | 5.0-6.0 | 1 to 5 | 10 | 8 |
| LM29 | 30 | 40-60 | 2.0-4.0 | >6 | 1 to 5 | 10 | 8 |

As only one parameter was varied at a time the other variables were fixed to the default settings shown in Table 5.6.

**Table 5.8**: Results for extruder variables

| Sample | Density (kg/m^3) | Porosity | Flow resistivity (N.s.m^-4) | Parameter changed |
|---|---|---|---|---|
| **LM10** | 366 | 0.75 | 14,200 | Binder level 10% |
| **LM11** | 310 | 0.77 | 12,600 | Binder level 20% |
| **LM12** | 245 | 0.84 | 11,300 | Binder level 30% |
| **LM13** | 220 | 0.87 | 8,800 | Binder level 40% |
| **LM14** | 180 | 0.88 | 8,100 | Binder level 50% |
| **LM15** | 168 | 0.89 | 6,200 | Fibre:Grain (20:80) |
| **LM16** | 159 | 0.92 | 5,400 | Fibre:Grain (40:60) |
| **LM17** | 193 | 0.86 | 6,600 | Fibre:Grain (60:40) |
| **LM18** | 226 | 0.8 | 7,200 | Fibre:Grain (80:20) |
| **LM19** | 241 | 0.74 | 8,200 | Fibre:Grain (100:0) |
| **LM20** | 154 | 0.91 | 8,700 | Grain size <0.5 mm |
| **LM21** | 171 | 0.88 | 9,100 | Grain size 0.5-1.0 mm |
| **LM22** | 196 | 0.86 | 9,200 | Grain size 1.0-2.0 mm |
| **LM23** | 202 | 0.85 | 10,200 | Grain size 2.0-4.0 mm |
| **LM24** | 229 | 0.82 | 10,500 | Grain size >5.0 mm |
| **LM25** | 205 | 0.76 | 8,600 | Fibre length <1 mm |
| **LM26** | 190 | 0.82 | 8,300 | Fibre length 2.0-4.0 mm |
| **LM27** | 176 | 0.86 | 7,800 | Fibre length 4.0-5.0 mm |
| **LM28** | 170 | 0.88 | 6,600 | Fibre length 5.0-6.0 mm |
| **LM29** | 162 | 0.94 | 5,300 | Fibre length >6 mm |

Experimental results given in Table 5.8, suggest that the density, porosity and flow resistivity of the extruded samples made from recycled PVC backed carpet tiles are dependent on all the parameters changed, e.g. binder level, fibre to grain ratio, grain size, fibre length. During the extrusion process the porosity can change considerably from 74% to 94% as $CO_2$ gas is released during the reaction.

The binder has a big influence on the density, porosity and the flow resistivity; this is an expected result, since using low levels of binder increases the density of the material reducing the porosity, the opposite is true with higher levels of binder.

Figure 5.9 illustrates the influence of binder (XP2261) that foams more than other binders used in the previous experiments. The effect of binder level is more pronounced when using binders with low boiling point foaming agents and the 4 4' MDI isomer. Binder (XP2261) used for this set of experiments was from Chemique adhesives; this binder produced low density materials (Table 5.9). In Figure 5.9, the sudden change in porosity is noticed at around 30% binder level, 5% n-pentane was also added to the mix to increase further the porosity because n-pentane has a low boiling point during the exothermic reaction the n-pentane liquid boils creating more pores in the structure hence the materials porosity increases.

**Table 5.9**: Influence of binder (XP2261)

| Sample | Binder (%) | Flow resistivity ($N.s.m^{-4}$) | Porosity (%) | Density ($kg/m^3$) |
|---|---|---|---|---|
| ES30 | 10 | 60,446 | 89.2 | 198 |
| ES31 | 20 | 35,456 | 91.8 | 110 |
| ES32 | 30 | 6,513 | 93 | 105 |
| ES33 | 40 | 3,782 | 97.1 | 53 |
| ES34 | 50 | 3,479 | 98.5 | 34.4 |

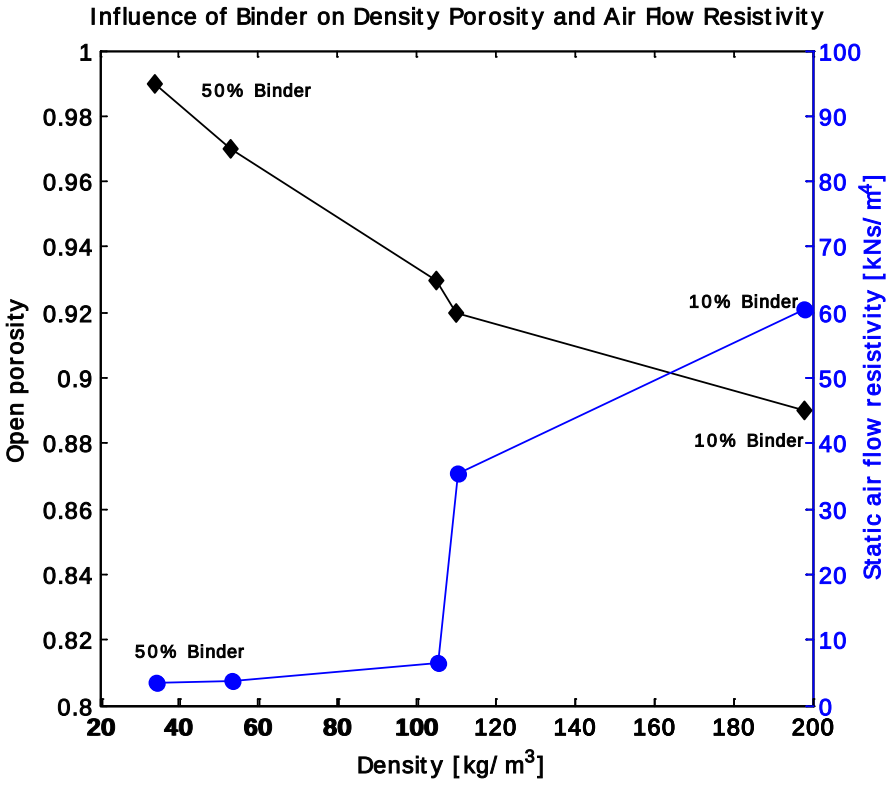


**Figure 5.8**: Influence of binder (XP2261) levels on porosity and flow resistivity

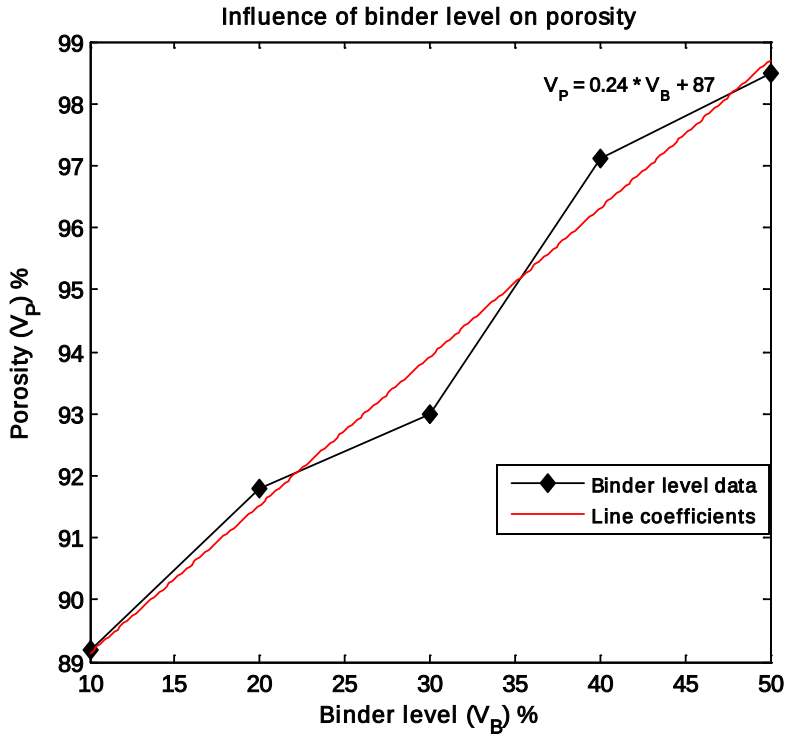


**Figure 5.9**: Sudden change in porosity at 30% binder level

Influence on porosity of binder from Rosehill Polymers (FX1109) is presented in Figure 5.10, the results show that the density decreases with increasing binder levels.

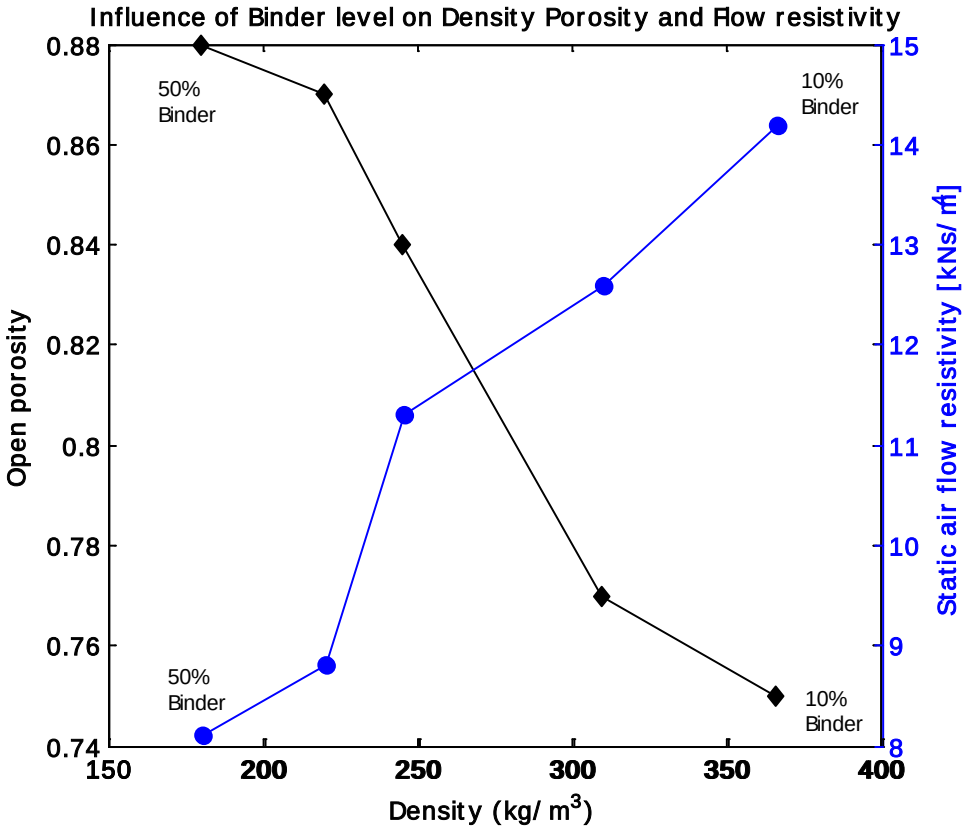


**Figure 5.10**: Influence of binder (FX1109) levels on porosity and flow resistivity

It can clearly be seen in Figure 5.10 the influence of binder on the flow resistivity and open porosity is measurable.

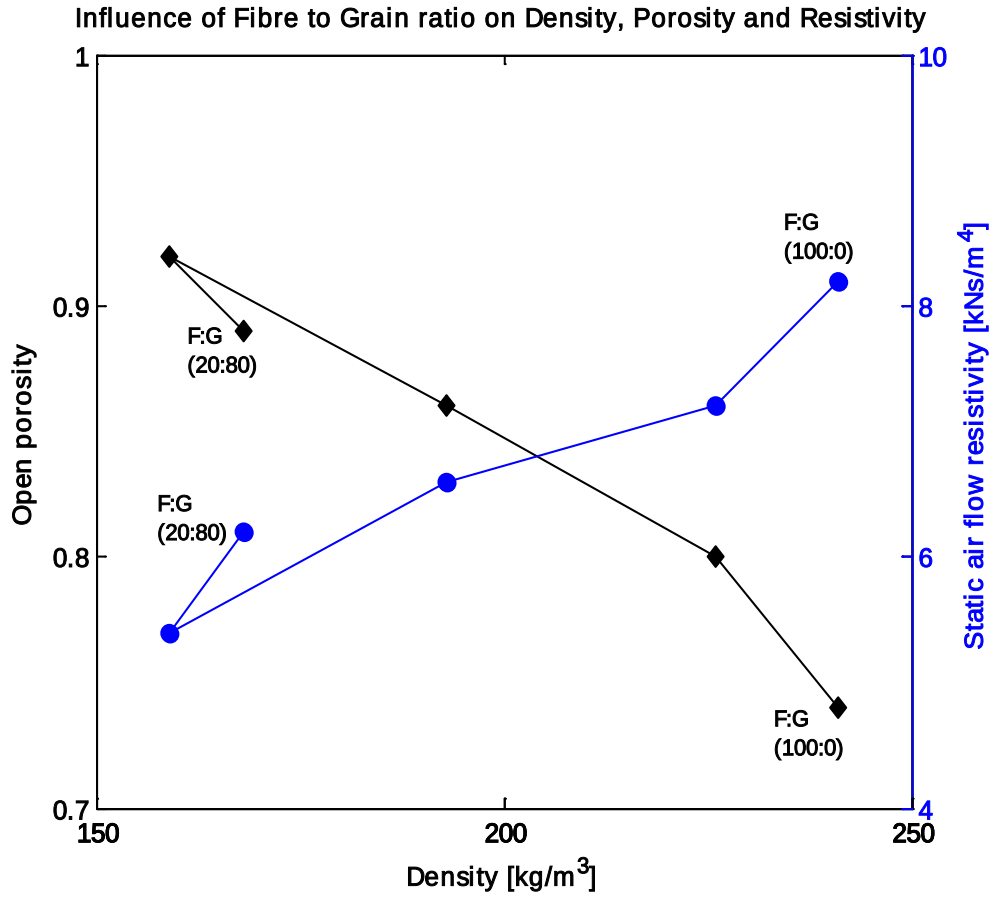


**Figure 5.11**: Influence of fibre to grain ratio on porosity and flow resistivity

The general behaviour of the graph shown in Figure 5.11 suggests that the porosity increases with higher grain levels while the flow resistivity decreases. The jump in the data for F:G (20:80) is due to the collapsing of the foam during the reaction because the sample was unable to support the quantity of grains, a point also to note is that fibres are lighter than grains in density.

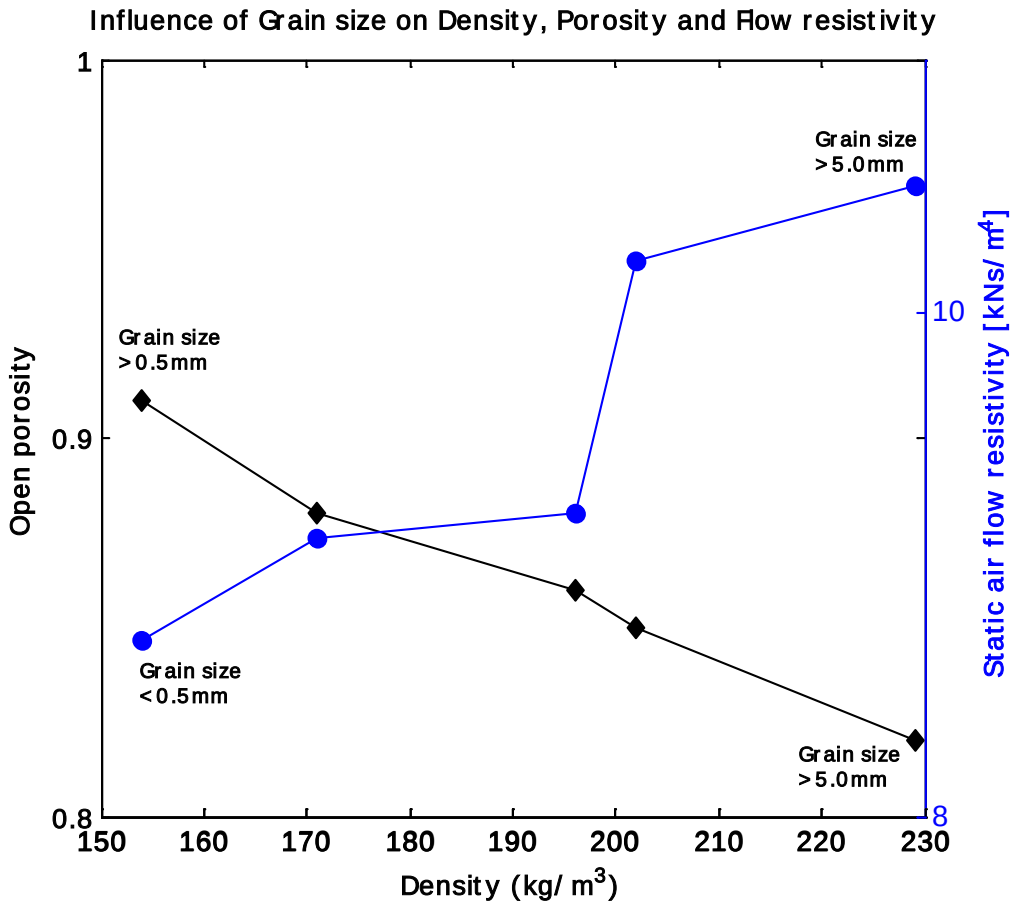


**Figure 5.12**: Influence of grain size on porosity and flow resistivity

It can be seen in Figure 5.12 that the flow resistivity and the open porosity are not influenced to a great extent by the grain size. One possible explanation for the jump in the flow resistivity between the material samples made from 1 to 4 mm diameter grains could be due to the inhomogeneity in the material produced.

Although fibre to grain ratio, grain size and fibre length affect the density (Figure 5.11-13), they do not necessarily result in any significant variation of the flow resistivity, the results show that the flow resistivity begins to increase almost linearly with density.

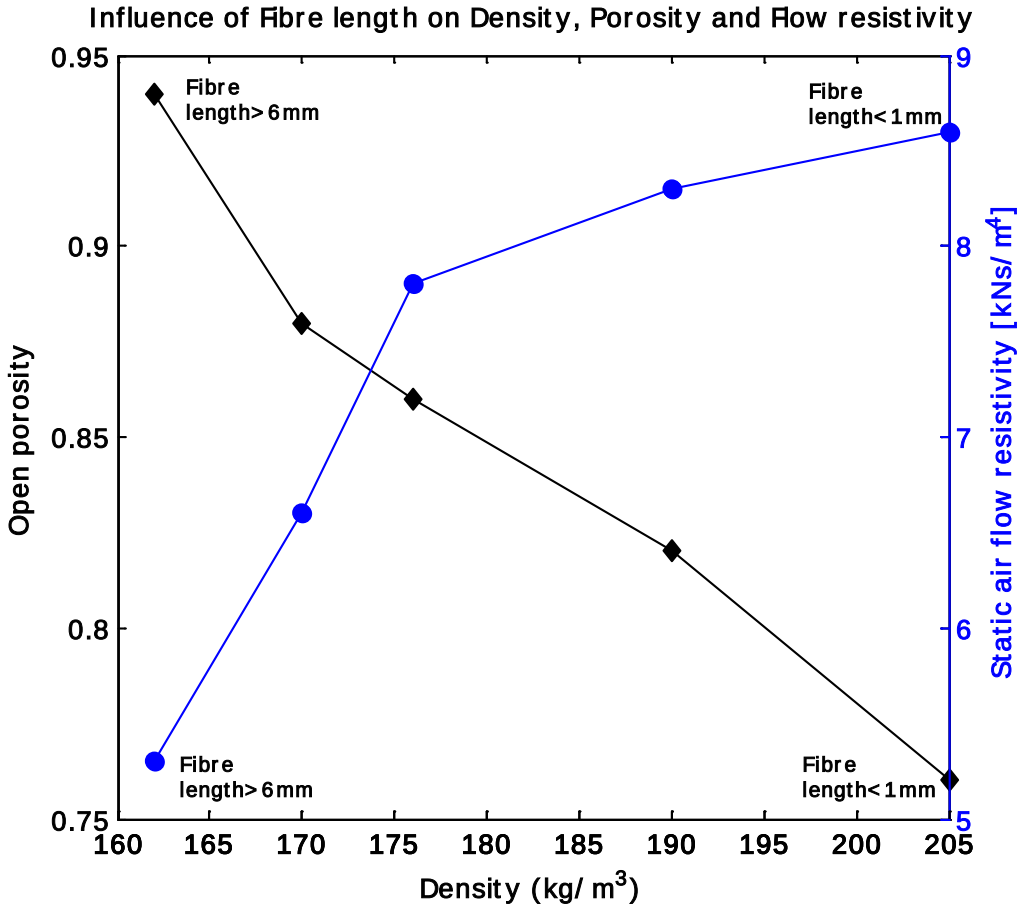


**Figure 5.13**: Influence of fibre length on porosity and flow resistivity

The trend in porosity and air flow resistivity curves are observed for various fibre to grain ratios, binder levels, fibre length and grain size, which are attributed to changing the extruder variables which affect the density of the sample. It is clear that the key features that control porosity are higher binder concentrations; and an approximately equal fibre to grain ratio. Therefore, by changing the extruder variables the chemistry of the extrudate can be controlled to deliver high porosity and optimal air flow resistivity values. In this way the non-acoustic properties of the extruded materials can be influenced by the extruder parameters through the control of the pore size distribution, porosity and air flow resistivity to achieve a good noise control performance.

## 5.5 Influence of extruder variables on sound absorption

Due to the complex structural morphology of the materials produced, a macroscopic indicator was chosen to study the acoustical performance of the extruded samples made from post manufacturing PVC carpet waste, the sound absorption coefficient at normal incidence measured by means of an impedance tube.

The influence of extruder variables on the plane wave normal incidence absorption coefficient for samples made from recycled PVC backed carpet tiles is shown in Figures 5.14 – 17. The extruder variables used in the experiments are presented in Table 5.7.

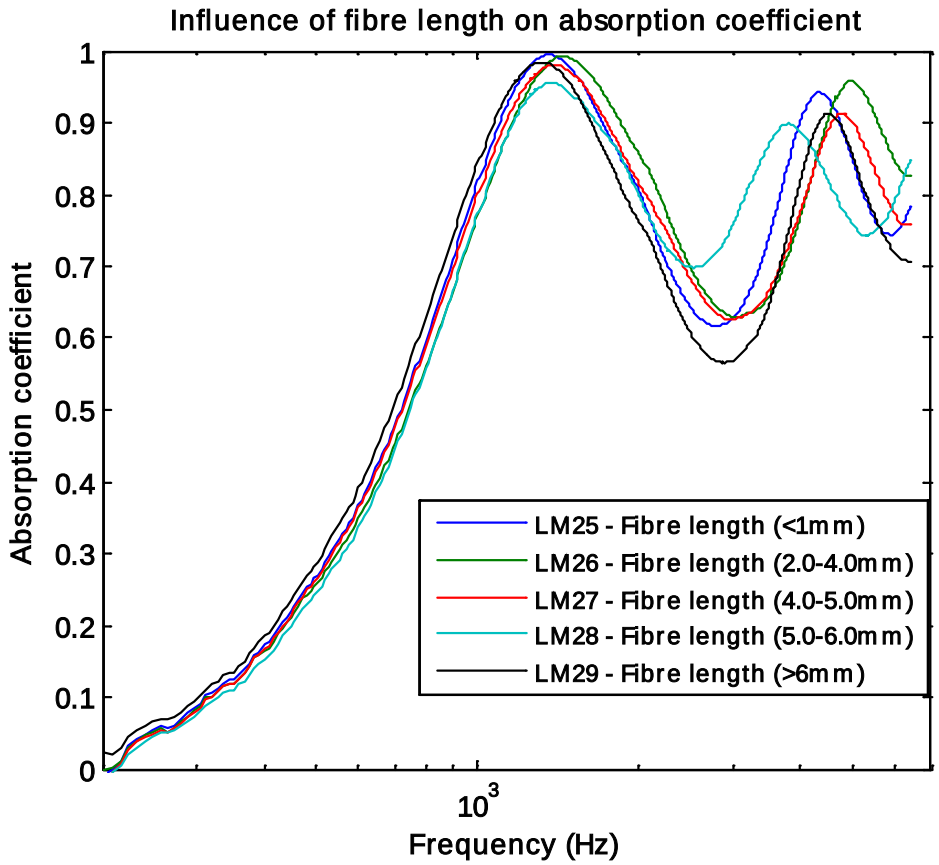


**Figure 5.14**: Influence of fibre length on sound absorption at normal incidence for samples having thickness of 30mm. All other variables were kept equal to the default values of table 5.6

Figure 5.14 presents the effect of fibre length on the acoustic absorption coefficient of the extruded materials. The results show that the fibre length does not have a strong effect on the absorption coefficient over the whole frequency range. The behaviour at higher frequencies may be attributed to material heterogeneities and the sample edge effect. It is likely that fibres become impregnated into the binder base frame and the effect of their length is small in comparison with that produced by the binder.

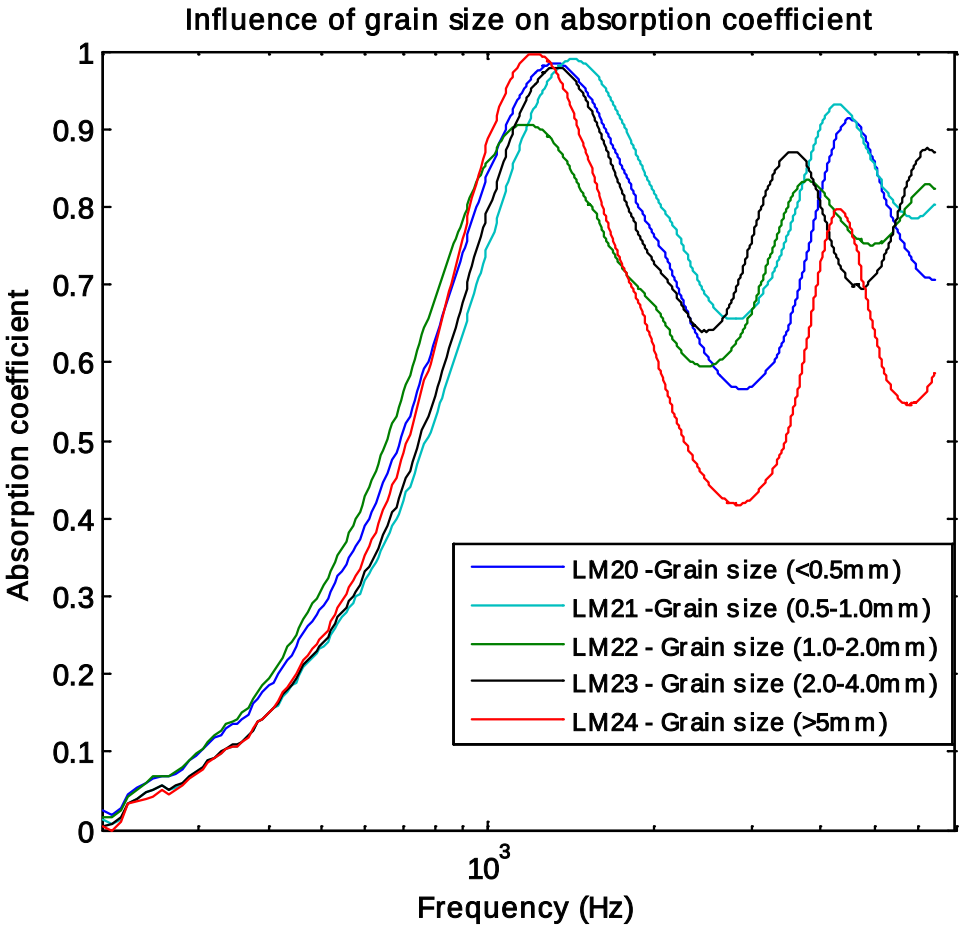


**Figure 5.15**: Influence of grain size on sound absorption at normal incidence for samples having thickness of 30mm. All other variables were kept equal to the default values of table 5.6

Figure 5.15 presents the sound absorption coefficient at normal incidence of 30 mm thick samples manufactured with different grain sizes. All other variables were kept to the default values as suggested in Table 5.6. The absorption coefficient for the materials is similar below 1000 Hz. Above this frequency the behaviour of the absorption coefficient seems to depend on the grain size and materials made of smaller grain size tend to absorb better.

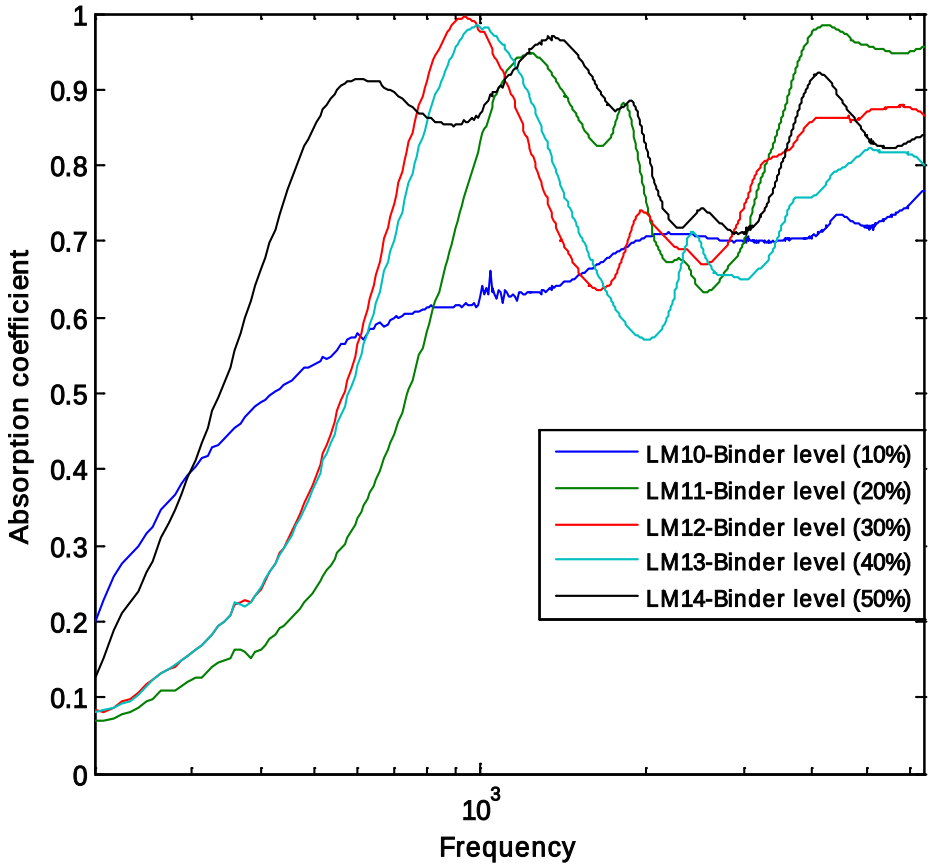


**Figure 5.16**: Influence of binder (FX1109) on sound absorption at normal incidence for samples having thickness of 30mm. All other variables were kept equal to the default values of table 5.6

Figure 5.16 presents the effect of the binder level on the acoustic absorption coefficient of the extruded materials. The results suggest that the influence of binder level is more obvious compared to that in the case of variable fibre or grain size. Samples made with PVC backed carpet tiles using 10% binder level exhibit a relatively poor absorption coefficient compared with that achieved in the case when higher levels of binder were added to the system. Generally, higher binder levels result in better quality absorbers. On the other hand, the effect of binder is rather complex. A small reduction in binder concentrations can result in a large change in the achieved absorption coefficient (e.g. from 10% to 20%). The behaviour of the absorption coefficient suggests that there is a rather complex (non-normal) pore size distribution which results from the binding process. The results presented in Figures 5.14 - 5.16 also suggest that the nature of waste used in the extrusion process does not have a strong effect on the absorption performance of the extruded samples. The absorption in these materials is mainly controlled by the binder type and level. Specifically, the binder type is critical as illustrated in Figure 5.8 and 5.16 where different types of binder were used in the production process.

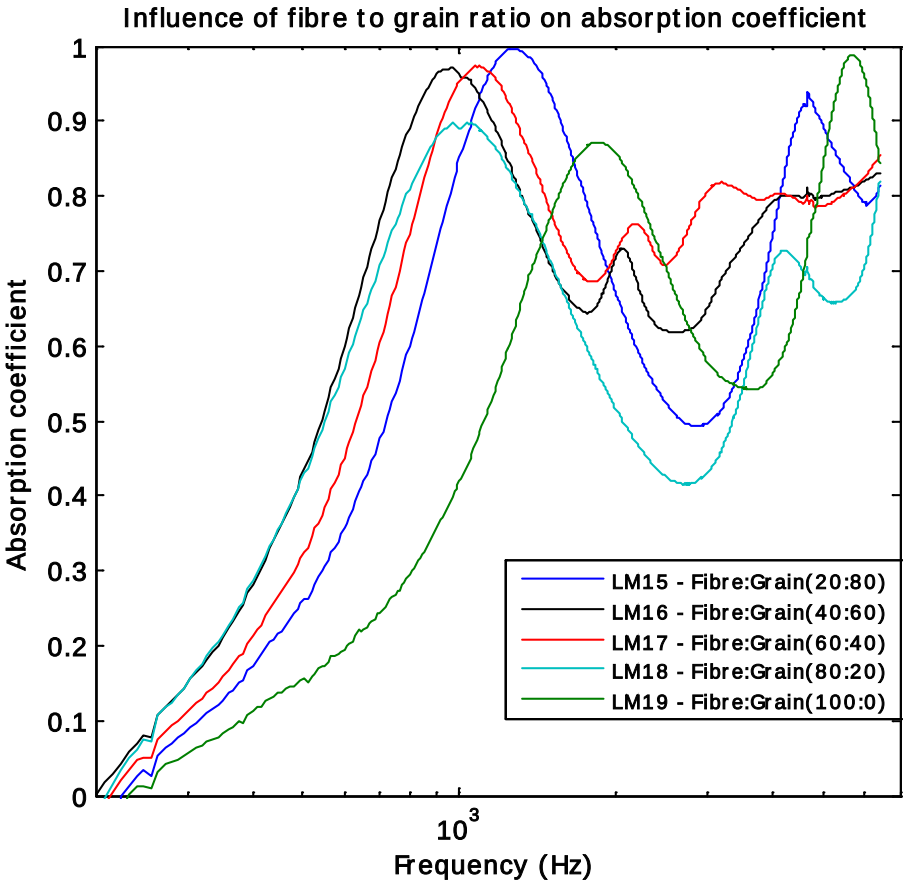


**Figure 5.17**: Influence of fibre to grain ratio on sound absorption at normal incidence for samples having thickness of 30mm. All other variables were kept equal to the default values of table 5.6

Figure 5.17 presents the absorption coefficient for material samples produced using post manufacturing carpet waste with variable grain to fibre ratios. It is clear from the results presented in this figure, that if no grain matter is present in the material, then the absorption coefficient is relatively low, the porosity is relatively low and the flow resisitivity is relatively high (see Table 5.8). The best results were achieved when ratios of fibre to grain were 40:60 or 60:40. Thus an approximately equal amount of these components were needed to achieve high absorption coefficient. It is also interesting to

note that 40:60 ratio of fibre to grain is present in the original PVC backed carpet tiles before granulation so that no special separation is required for this particular waste stream.

Based on the assessment of the extruder variables it is clear that the key features that drive absorption performance when considering how to deliver a good performance are shorter fibre length, smaller grain size, high binder level and approximately equal fibre to grain ratio. Therefore, by changing the extruder parameters the chemistry of the materials can be changed to deliver high porosity and optimal air flow resistivity values needed for good quality acoustical absorbers.

## 5.6 Experiments using the larger modified extruder

Further trials with the larger modified extruder were carried out using car dashboard crumb (obtained from recycling Jaguar cars) and rayon (tyre shred residue waste). In the experiments, the extrusion screw speed was set to give a dry solid flow rate of 40 kg/h. The material was extruded, collected in trays and allowed to set for a sufficient time. The results for materials extruded with varying binder levels are presented in Table 5.8 for tyre shred residue (rayon) and car dashboard crumb. The single number rating for sound absorption for rayon material is similar for all binder levels (see Table 5.10). For materials made using car dashboard crumb the single number rating for sound absorption is better in the case of the lower levels of binder.

**Table 5.10**: Acoustic and other characteristic data for the extruded materials

| Material | Fibre length (mm) | Density ($kg/m^3$) | Porosity (%) | Flow resistivity ($N.s/m^4$) | Dynamic Stiffness (Pa/m) ($x10^7$) | Impact Insulation Broadband (dB) | Sound Abs. (DLa,) |
|---|---|---|---|---|---|---|---|
| Rayon (50%) | 1-3 | 145.7 | 89.6 | 8,050 | 2.9 | 130 | 3 |
| Rayon (40%) | 1-3 | 299 | 77 | 8,600 | 2.93 | 132 | 3 |
| Rayon (30%) | 1-3 | 345 | 72 | 8,900 | 2.97 | 132 | 3 |
| Rayon (20%) | 1-3 | 370 | 71 | 9,100 | 3.19 | 133 | 4 |
| Rayon (10%) | 1-3 | 495 | 67 | 10,200 | 3.21 | 135 | 3 |
| Dashboard (Gray-50%) | Grain Size 1-10 | 247.4 | 78.3 | 8,065 | 3.6 | 133 | 2 |
| Dashboard (Gray-40%) | Grain Size 1-10 | 300 | 72.5 | 9,500 | 3.71 | 135 | 2 |
| Dashboard (Gray-30%) | Grain Size 1-10 | 318 | 71.9 | 12,200 | 3.84 | 136 | 3 |
| Dashboard (Gray-20%) | Grain Size 1-10 | 363 | 70 | 13,000 | 3.97 | 137 | 3 |
| Dashboard (Gray-10%) | Grain Size 1-10 | 658 | - | - | - | - | - |

An important acoustical property of the extruded porous materials is the capability to insulate against the transmission of impact sound. In order to study the impact sound

insulation performance in underlay applications, the extruded material samples were subjected to a standard test with accordance to the Building Regulations Approved Document E (2003). The samples were tested using the instrument discussed in chapter 4, section 4.9. Comparison of the results of the extruded samples with the top commercial material (cloud 9) for impact sound insulation is shown in Figure 5.18 for samples 10mm thick.

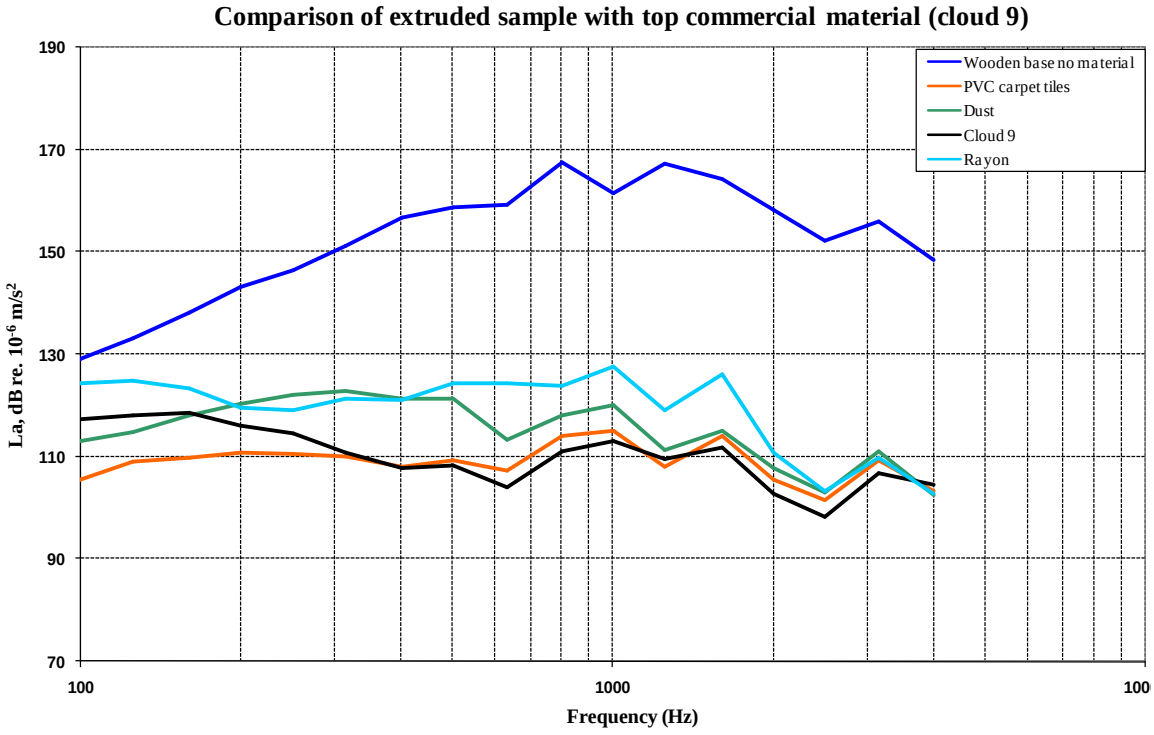


**Figure 5.18**: Comparison of impact sound insulation performance of extruded materials with a top commercial material

An indication of the acoustic performance of the underlay is obtained by comparing the octave band acceleration spectra between 100 and 4000 Hz. The lower the amplitude of the transmitted vibration acceleration, the better performing is the sample under test in

terms of its impact sound insulation performance. The impact sound insulation results in Figure 5.18 show the performance of sample made using PVC backed carpet tiles to be similar to the commercial material Cloud 9. For comparison purposes impact testing with no underlay sample attached to the impact rig was carried out by dropping the mass directly onto the bare timber.

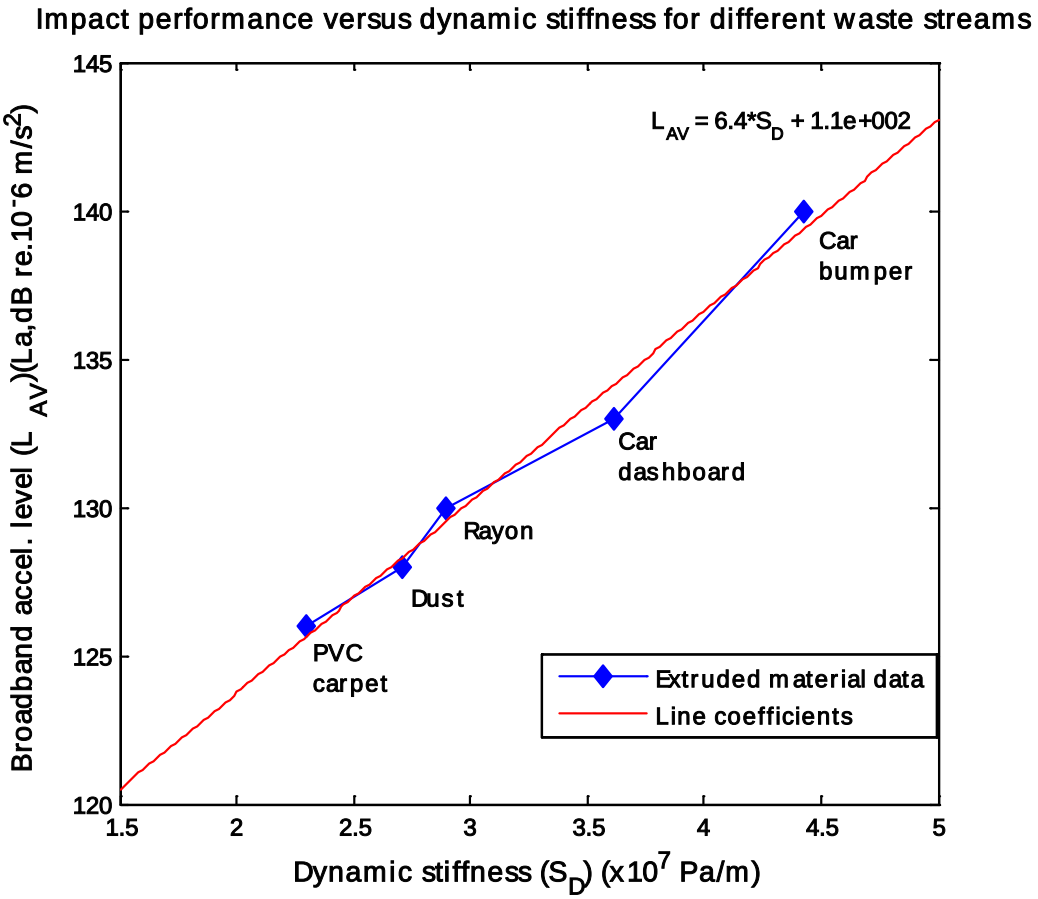


**Figure 5.19**: Impact performance of different waste streams versus dynamic stiffness

Figure 5.19 shows impact performance against the measured values of the dynamic stiffness. In terms of the broadband acceleration levels, the sample of PVC backed carpet tiles performs 2 dB better than the sample made of dust waste and dashboard and

by 7 dB better than that made from recycled bumpers granulates. The better performance of sample made of PVC backed carpet tiles are attributed to the differences in material stiffness and composition. The presented mean acceleration levels were determined by equations (4.36) and (4.37) presented in chapter 4.

Samples made from PVC carpet waste were tested for impact sound insulation and sound absorption; the samples produce adequate impact sound insulation and sound absorption to be able to compete confidently against the top commercial materials. Materials manufactured for impact sound insulation test were less porous but considerably more resilient using binder FX1199. From the experiments carried out so far it can be concluded that the extruded samples could be applied to achieve both excellent noise absorption and impact sound insulation.

## 5.7 Acoustic characterisation of the porous materials

Theoretical models were used to predict the acoustic absorption performance of the developed porous materials (Figures 5.20-21). The models were also used to determine the degree of inhomogeneity and variability in the key non-acoustical properties.

**Figure 5.20**: Picture of low density material made using tyre shred residue waste (YL01), formulation summary is given in appendix D

**Figure 5.21**: Picture of low density material made from carpet waste (ES10), formulation summary is given in appendix D

By testing six specimens cut from the same material, the mean and standard deviation in the acoustic absorption coefficient was calculated for each material to study the materials homogeneity. This data is illustrated in the following graphs. The pore size distribution in these materials was also measured and used to understand better the observed acoustical absorption performance. Figures 5.22 to 5.36 show the influence of binder levels on the acoustic absorption coefficient and the corresponding pore size distribution of products made from recycled tyre shred residue. As the level of binder is increased the amount of meso-pores increase in the products. This is due to the higher level of $CO_2$ gas that is produced during the reaction of MDI binder with water.

Figure 5.22 and the following figures shows the influence of the binder level on the standard deviation (the gray area) of six samples taken from the same material tested top and bottom end all 30mm in thickness (±1mm).

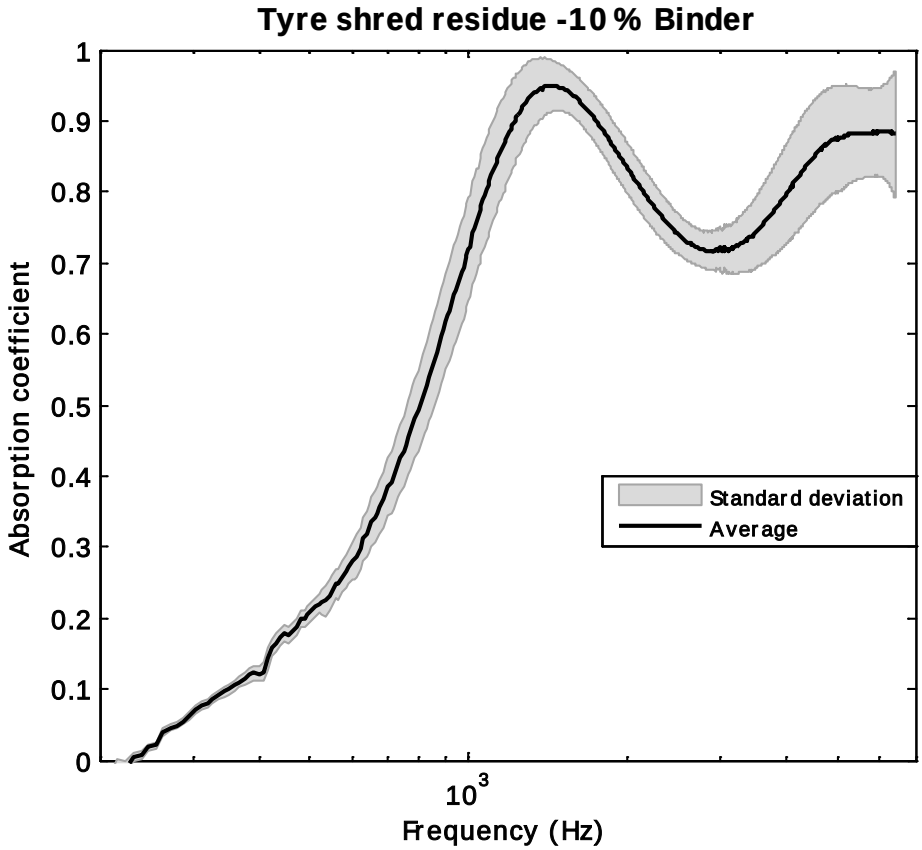


**Figure 5.22**: Absorption of tyre shred residue with 10% binder level

The porosity of the material made using 10% binder was 67%; the flow resistivity was 10,200 N.s/m$^4$. The pore size distribution shown in Figure 5.23 is between 0.04 to 1.12 mm. Due to these micro-pores the observed absorption coefficient is high, at 1000 Hz the absorption coefficient is ~ 0.7.

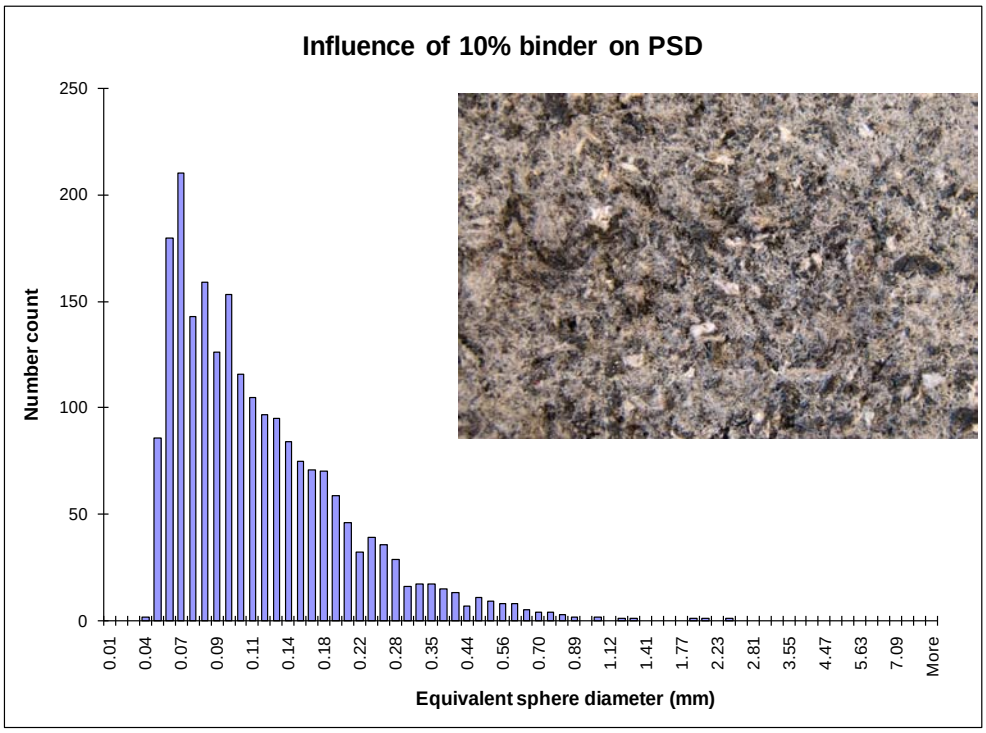


**Figure 5.23**: Pore size distribution for 10% binder

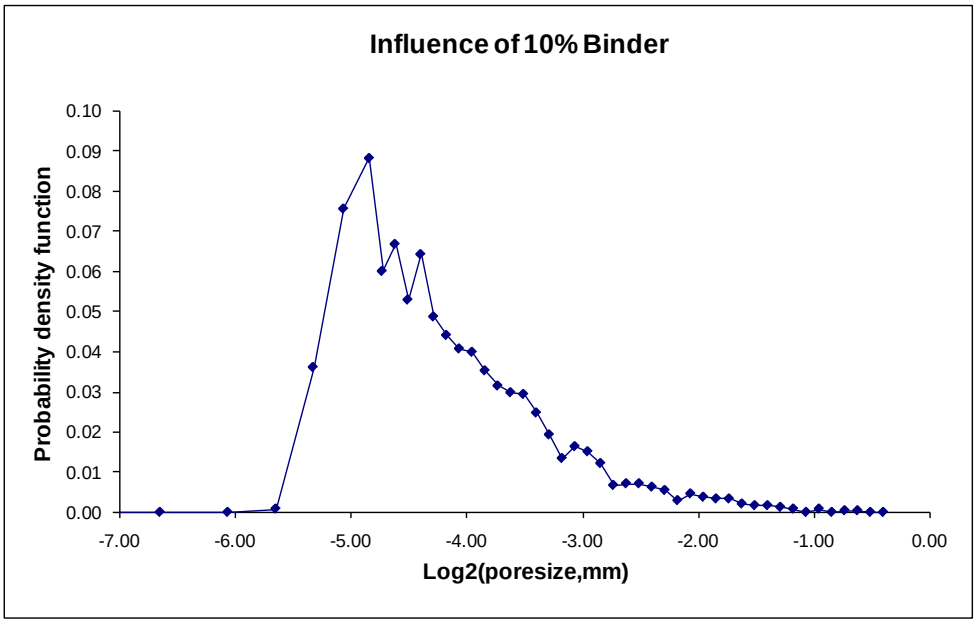


**Figure 5.24**: Probability density function for 10% binder

The ability of porous materials of limited thickness to absorb below 1000 Hz is rather useful because this is an important frequency range where a considerable amount of noise energy in concentrated. A wider pore size distribution has proved to help to improve the low frequency performance of porous materials of limited thickness (Only and Boutin, (2003)). Many of the extruded materials are characterised by a broad pore size distribution which should help to improve the low frequency performance. The acoustic absorption data presented here should substantiate this claim.

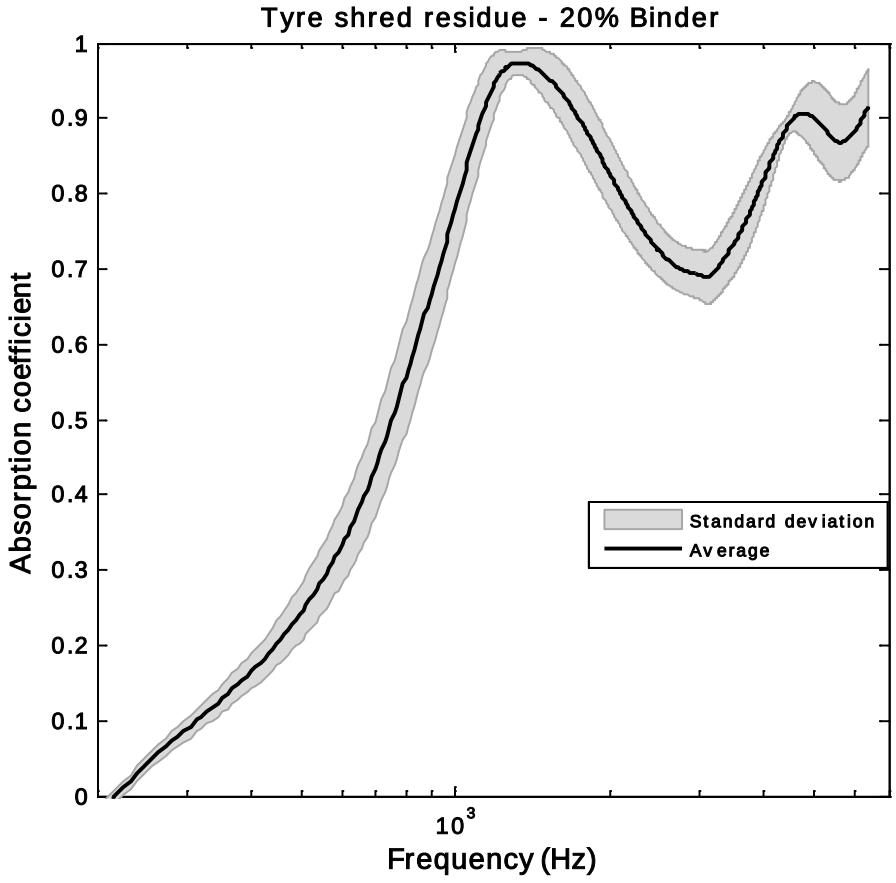


**Figure 5.25**: Absorption of tyre shred residue with 20% binder level

The porosity of the material made using 20% binder was 71%; the flow resistivity was 9,100 N.s/m$^4$. The pore size distribution shown in Figure 5.27 is between 0.04 to 6 mm,

due to this combination of micro-pores and meso-pores the observed absorption coefficient is high at the lower frequencies, at 1000 Hz the absorption coefficient is ~ 0.8.

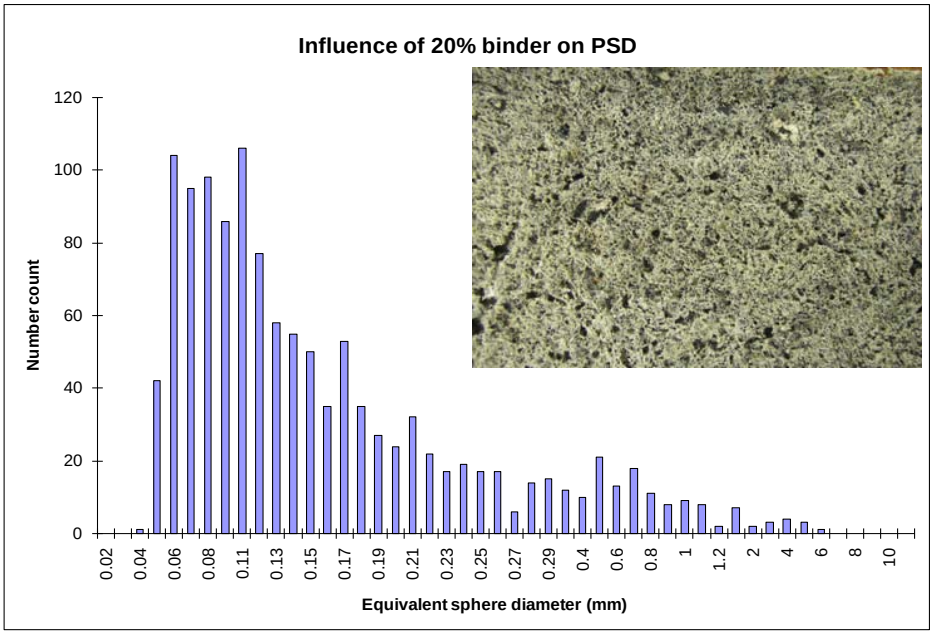


**Figure 5.26**: Pore size distribution for 20% binder

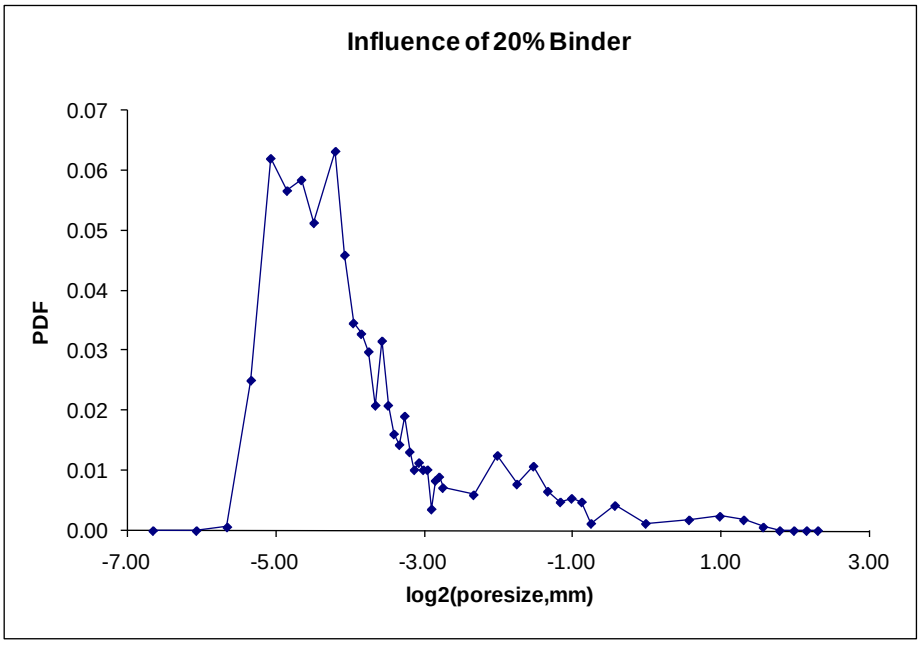


**Figure 5.27**: Probability density function for 20% binder

It is clear from the single rating values (Table 5.12) for absorption coefficient with 20% binder yields the highest absorption coefficient values for materials made of tyre shred residue. This is attributed to the pore size distribution which peaks around 100μm (see Figure 5.26) and the high porosity of 71%. This pore size is typical in good quality acoustic fibreglass.

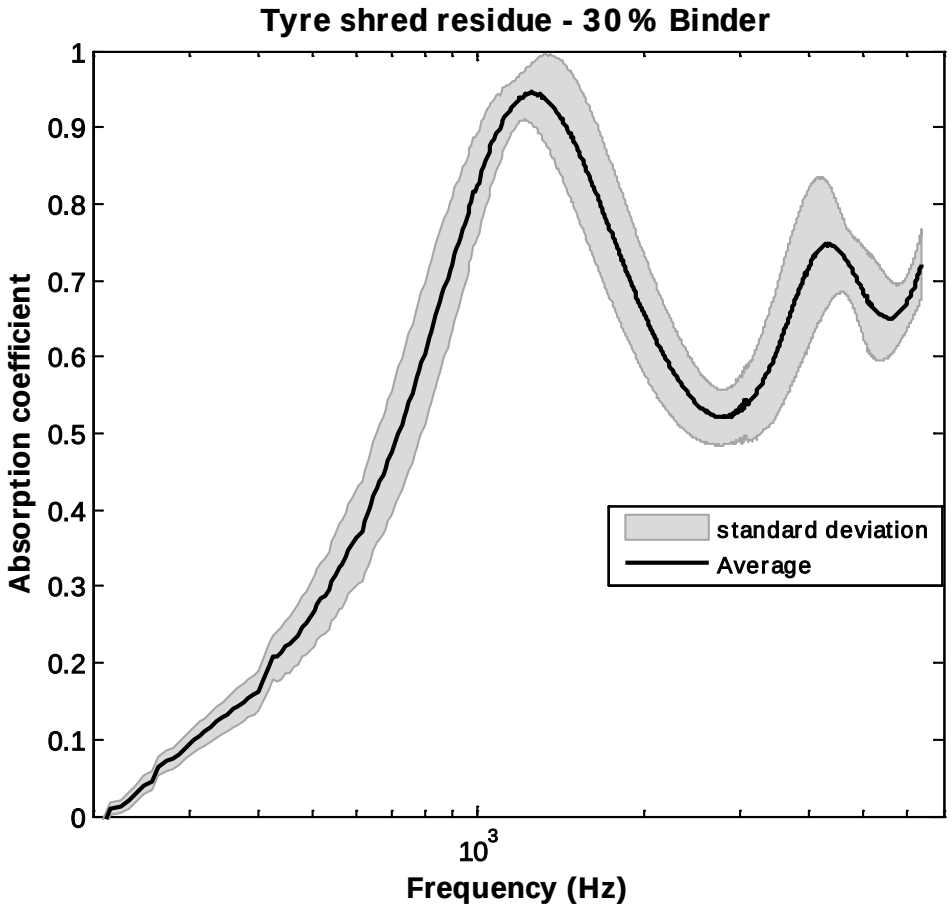


**Figure 5.28**: Absorption of tyre shred residue with 30% binder level

The porosity of the material made using 30% binder was 72%; the flow resistivity was 8,900 N.s/m$^4$. The pore size distribution shown in Figure 5.29 is between 0.04 to 8 mm,

due to this combination of micro-pores and meso-pores the observed absorption coefficient is high, at 1000 Hz the absorption coefficient is ~ 0.8.

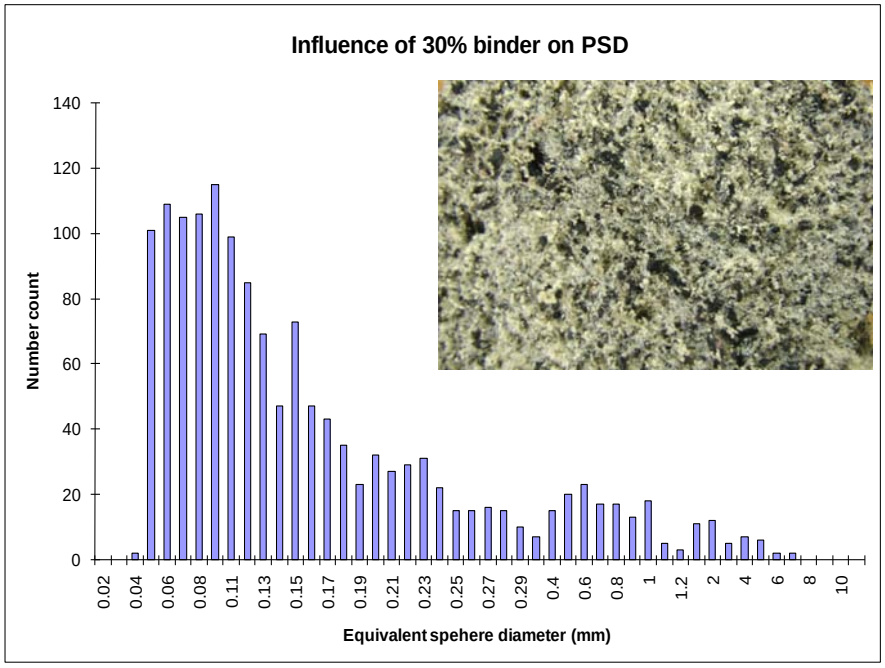


**Figure 5.29**: Pore size distribution for 30% binder

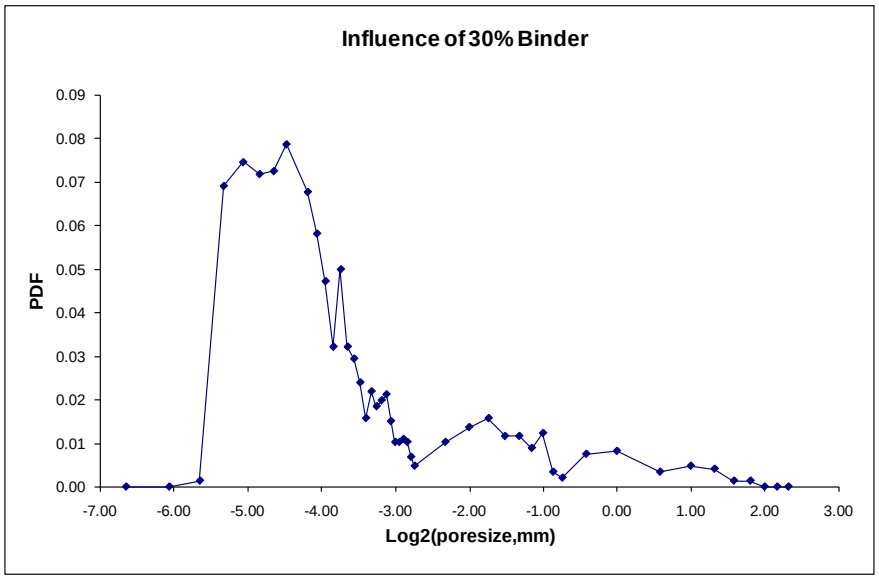


**Figure 5.30**: Probability density function for 30% binder

An increase in the binder level from 20% to 30% resulted in a noticeable reduction of the absorption coefficient in the higher frequency range (Figure 5.28), throughout the spectrum for materials made of tyre shred residue. The results suggest that similar increases in the binder level may not necessarily result in equal changes in the absorption coefficient. For example, the absorption coefficient is less sensitive to the variation in the binder levels in the range 10-20%. For higher binder levels the pore size ranges from 0.04mm to 8cm, as a result the flow resisitivity values are lower, standing waves can develop in the sample, therefore at higher frequencies the absorption coefficient spectrum can become very erratic.

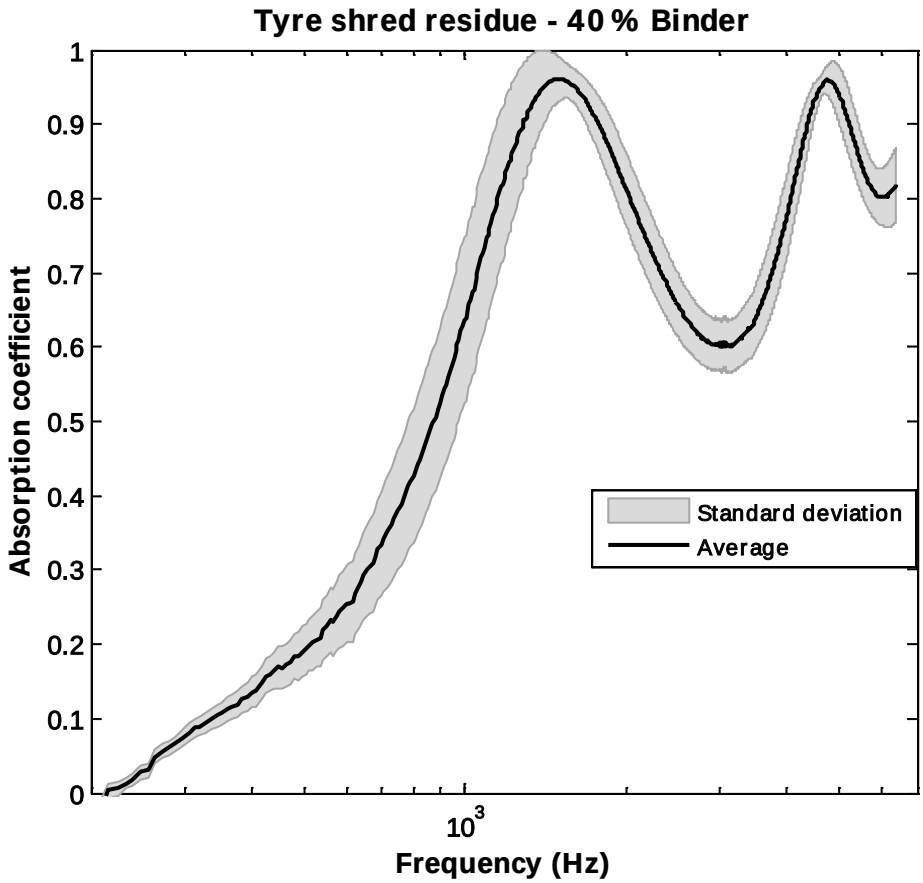


**Figure 5.31**: Absorption of tyre shred residue with 40% binder level

The porosity of the material made using 40% binder was 77%; the flow resistivity was 8,600 N.s/m$^4$. The pore size distribution shown in Figure 5.32 peaks around 0.13 mm, the observed absorption coefficient at 1000 Hz is ~ 0.6.

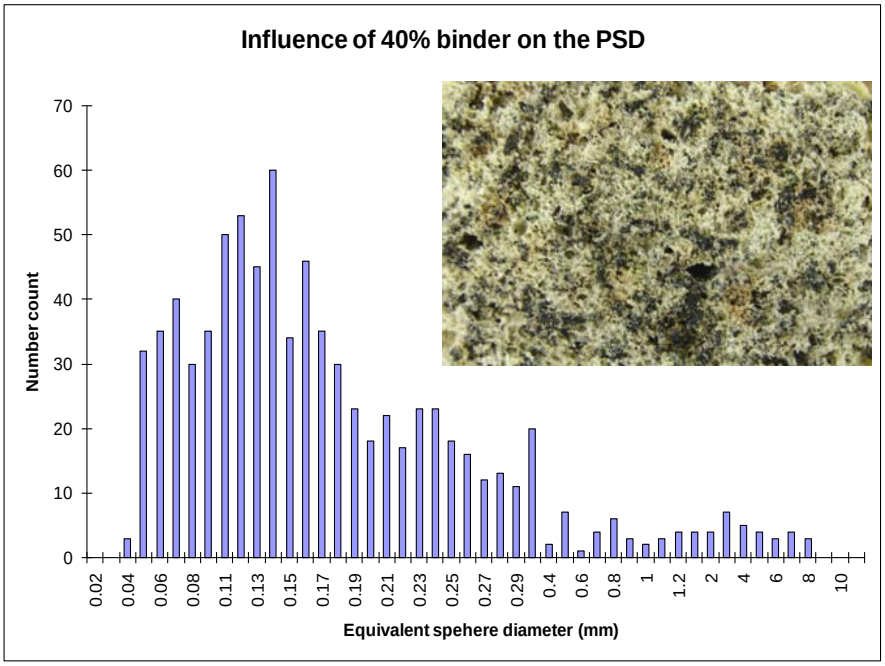


**Figure 5.32**: Pore size distribution for 40% binder

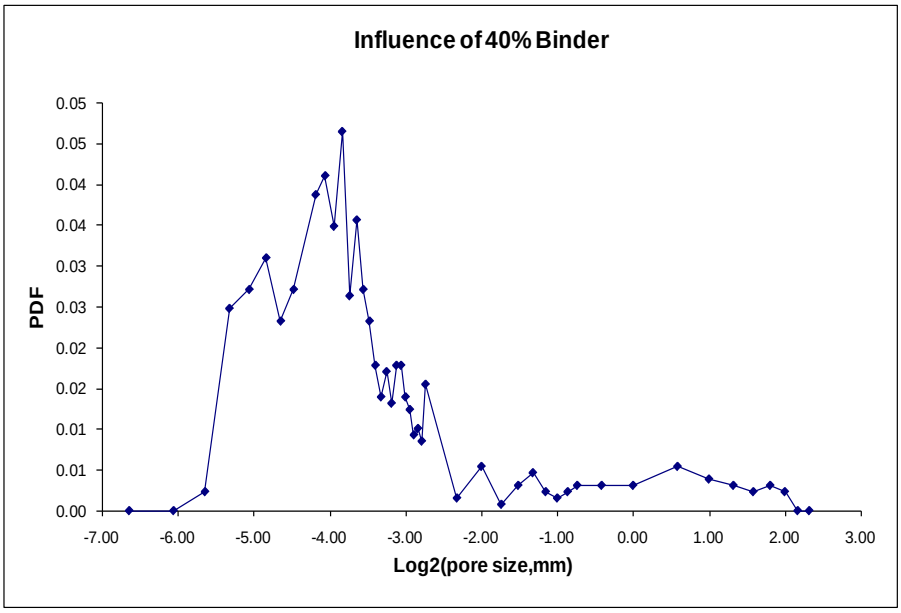


**Figure 5.33**: Probability density function for 40% binder

For 40% binder level the absorption coefficient for the samples reaches a peak value of above 0.9, and stays above 0.55 up to the impedance tubes cut-off frequency of 6.4 kHz. Normal incidence absorption results are a good indicator of performance under random incidence (real – life) conditions, so a high peak value for normal incidence absorption coefficient suggests that these samples are capable of achieving high values of the random incidence absorption coefficient. It is also possible to broaden the absorption coefficient peak and shift it to lower frequencies by increasing the sample thickness, if this is suitable or desirable for a given application. From the acoustic point of view the materials performance benefits from an extensive network of micro-pores and meso-pores created between individual grains and fibres.

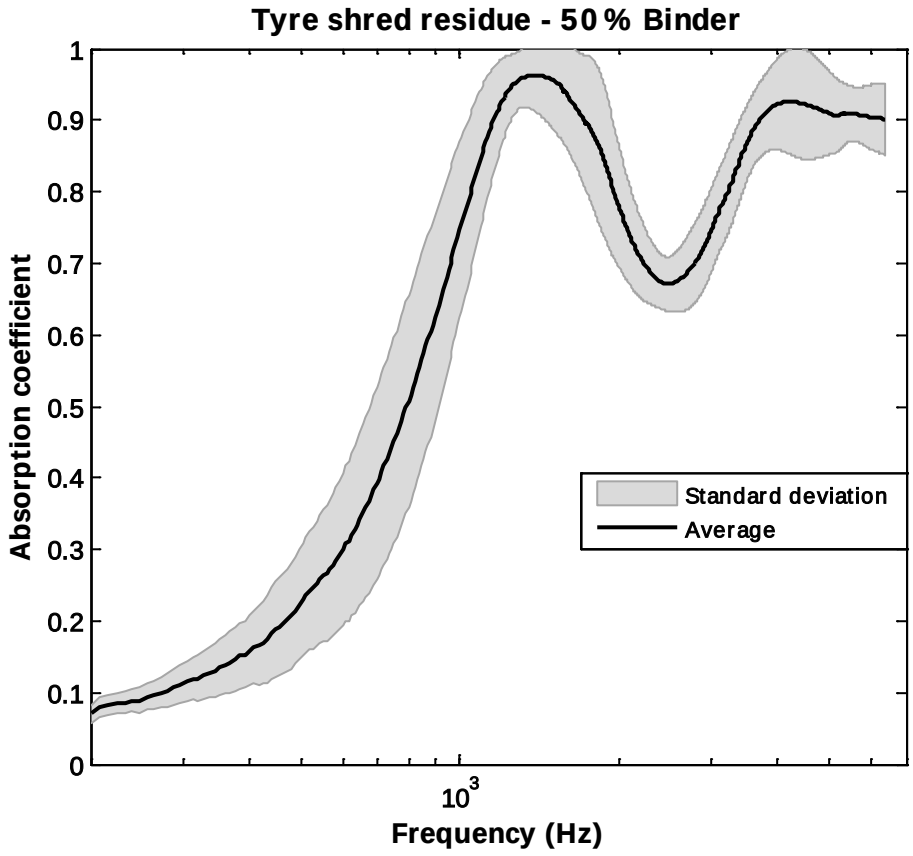


**Figure 5.34**: Absorption of tyre shred residue with 50% binder level

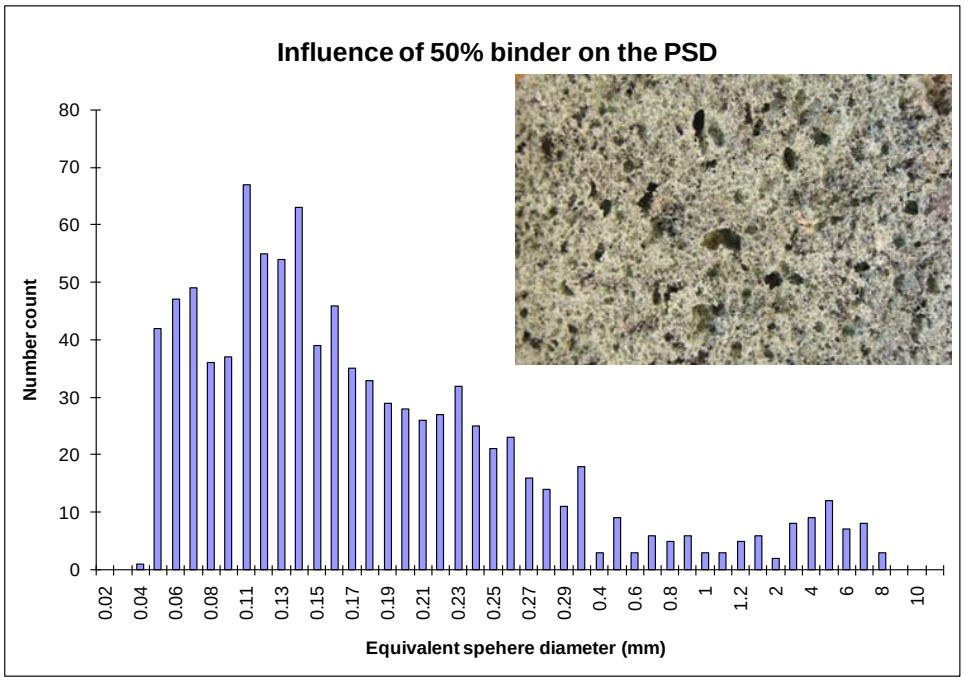


**Figure 5.35**: Pore size distribution for 50% binder

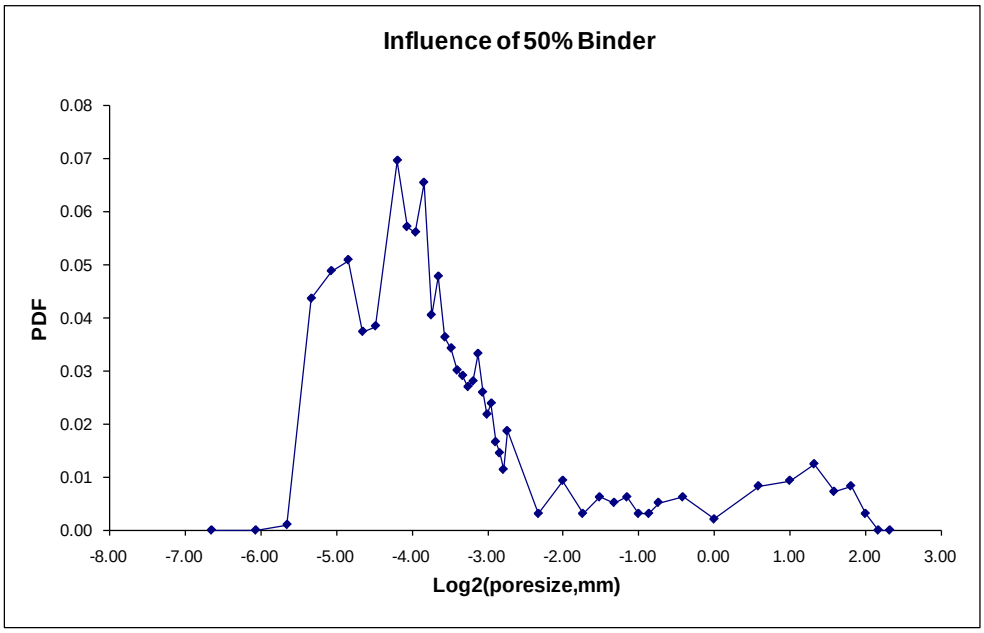


**Figure 5.36**: Probability density function for 50% binder

Comparing the 10% binder level graph (Figure 5.22) with the 50% binder level graph (Figure 5.34) it is evident that as binder level is increased the samples become less homogeneous. For lower levels of binder the standard deviation of the absorption coefficient is low in comparison with higher binder levels. It is clear from the results samples made using lower binder levels are more homogeneous. Materials which were produced with a high binder level were largely heterogeneous due to a number of meso-pores created within the porous structure.

The absorption coefficient of a material layer of a certain thickness depends on the internal characteristics of each sample such as flow resistivity, porosity, and pore size distribution. From a practical point of view, the acoustic energy penetrates into the sample only up to a certain depth, which depends on both wavelength (frequency) and flow resistively. From close examination of the optical analysis of the pore size distribution data (PSD), it can be argued that there is a middle region of pore sizes for which the value of PSD is relatively small (i.e. the region between 1 and 1.5 mm, Figure 5.35). This region was considered as the separating limit between the micro and mesopores. The minimum ratio between the characteristic dimensions of the meso and microporous parts was set to $l\_meso \,/\, l\_micro \approx 10$. PSD data can in principle be used to determine the macroscopic values of the porosity, tortuosity, and flow resistivity as explained in chapter 4, section 4.4. According to the expressions presented in the work by Olny and Boutin (2003), the porosities can be computed by the aforementioned optical technique by which the overall areas attributed to the micro and the meso-pores can be discriminated.

## 5.8 Summary

The acoustic performance of the extruded samples made from polymeric waste can be controlled by careful selection of the extruder variables, the flow rate in the barrel, the flow rate out of the hoppers, and the water and binder flow rates. The acoustic performance of the extruded materials is affected by changing the variables (e.g. binder level, water level and waste level). The porosity, flow resistivity are almost dependant. This effect provides a good opportunity to develop tailored materials in terms of flow resistivity and porosity.

For enhanced acoustic absorption, there is the need to increase the proportion of the open interconnected pores. For a good thermal insulation performance a high proportion of closed pores filled with low-conductivity gas is required. For enhanced vibration insulation performance, there is a need to produce a resilient porous structure with low compressional modulus and high vibration damping. Mixing and chemistry controlled by the design and speed of the screw and the pressure controlled by the design of the die were key control parameters.